Hindawi
Journal of Electrical and Computer Engineering
Volume 2022, Article ID 1944117, 10 pages
https://doi.org/10.1155/2022/1944117

Research Article

A Novel DC-Power Control Method for Cascaded Converter under DC Voltage-Imbalance Condition

Zhenglong Xia,[1] **Qifan Wu**,[1] **Zongbin Ye**,[2] **Dongsheng Yu**,[2] **Lanqiao Zhu**,[1] **and Wenhao Hu**[1]

[1]*School of Electrical Engineering and Automation, Jiangsu Normal University, Xuzhou, Jiangsu 221116, China*
[2]*School of Electrical and Power Engineering, China University of Mining and Technology, Xuzhou, Jiangsu 221008, China*

Correspondence should be addressed to Zhenglong Xia; 59546461@qq.com

Received 26 October 2021; Revised 18 February 2022; Accepted 5 May 2022; Published 31 May 2022

Academic Editor: Andrea Bonfiglio

This paper proposes an interphase power control algorithm (IPCA) and submodule power control algorithm (SPCA) based on state transition PWM (ST-PWM) for cascaded H-bridge inverter with unbalanced DC sources. In this method, the correction value helps control the interphase power distribution and submodule power distribution by directly modifying the duty cycle of each switching state. In order to achieve linear modulation, an in-depth analysis of ST-PWM is conducted. Combining ST-PWM and IPCA, balanced AC currents and accurate power control on DC side can be achieved with an unbalanced DC source. The proposed strategies are simulated using MATLAB/Simulink and tested on a five-level laboratory prototype. Simulation and experimental results demonstrate the advantage and effectiveness of the proposed algorithm.

1. Introduction

The cascaded H-bridge converter (CHB) has become an outstanding type of converter circuitry in the medium-voltage converter field due to its merits, such as low switching voltage stress, improved output waveform quality, and modular and extendible structure [1–5]. As a suitable topology for high power applications, the CHB has been widely researched and applied both in research and industries, such as renewable energy systems [6], high-voltage power AC transmission systems [7], and large-scale photovoltaic power plants [8].

The CHB suits large photovoltaic power plants by providing separate DC links to photovoltaic (PV) strings and has better scalability to reach high power ratings. Therefore, the cascaded H-bridge converter is particularly attractive for photovoltaic grid-connected applications [8–11]. However, when the CHB serves as the interfacing converter for a PV system, the submodules will generate different power and DC voltages. This imbalance is mainly caused by nonuniform solar irradiances, unequal temperature, or inconsistent module degradation of different solar panels [11]. Unequal voltages and output power of DC sources in each submodule make the output voltage seriously distorted and lead to unbalanced AC current flowing to the grid, which could potentially make the whole system disconnected from the grid [10, 11]. Similar imbalance problems can be found in electric vehicles (EV) applications and energy storage systems [12]. In the electric vehicle applications [13, 14], for instance, the CHBs with batteries powering the vehicles are not equal and will vary while in use [15]. Because of the different characteristics of battery packs, unequal DC voltages become inevitable. This will result in unbalanced output power in electric vehicle [14]. But, with effective measures when the fault battery pack is cut off, the entire system can still work well. It is therefore essential to design suitable control strategies to tackle power imbalance problems.

In [16], a power balancing method is introduced to regulate the actual power transmitted through the dual active bridge (DAB) parallel modules. With this power balance control method, the current and power transmitted through each DAB module can be balanced. In [8], a distributed maximum power point tracking (MPPT) control method is proposed to increase the efficiency of PV systems. Therein, a control scheme with modulation compensation is

also proposed to acquire a balanced grid current under power imbalance conditions. In [10, 11], a fundamental frequency zero-sequence injection (FFZSI), double min-max (DMM), and double 1/6 third harmonic injection (DTHI) are proposed to balance the interphase power and grid current. There are mainly three drawbacks to the above methods: (1) the trigonometric calculations are complicated, and this might lead to overflow issues; (2) methods based on FFZSI might be ineffective when the power generation ratios are approximately equal; and (3) the relationship between the linear modulation index and power generation ratio limitation is unclear, which is important for PV systems under different modulation indexes. Moreover, these methods only analyze the adaptability in PV systems under equal DC sources but do not provide an efficient solution for CHB systems with unbalanced DC sources.

To solve the power imbalance problem for CHBs with unbalanced DC sources, in this paper, we propose an interphase power control algorithm (IPCA) and submodule power control algorithm (SPCA) based on state transition PWM (ST-PWM), to realize accurate power control for CHB with unbalanced DC sources. The power generation ratios per phase can be maintained to their expected value precisely by modifying the correction value derived from the two power control algorithms. Balanced AC currents at the AC side and accurate power control performance on the DC side are acquired with the proposed algorithms when the CHB operates under unbalanced DC sources, even under severe voltage-imbalance conditions.

2. Proposed Modulation Strategy with Unbalanced DC Sources

2.1. Introduction of the Simplified PWM Strategy under Unbalanced DC Sources. A typical CHB converter is shown in Figure 1, where $U_{\mathrm{dc\_}Xn}$ ($n = 1, 2, 3, \ldots$) represents the DC-source voltage of each submodule. The terminal voltage of each submodule is $U_{\mathrm{dc\_}Xn}$ in the P state, $-U_{\mathrm{dc\_}Xn}$ in the N state, and 0 V in the O state. $U_{\mathrm{dc\_A}}$, $U_{\mathrm{dc\_B}}$, and $U_{\mathrm{dc\_C}}$ stand for the total DC-source voltage per phase.

$$U_{\mathrm{dc\_}X} = \sum_{1}^{n} U_{\mathrm{dc\_}X_n} (X = A, B, and C). \tag{1}$$

$U_{\mathrm{dc\_ave}}$, the average value of $U_{\mathrm{dc\_Xn}}$, is expressed as (2). r_X in (3) stands for the interphase voltage-imbalance coefficient.

$$U_{dc\ \_ave} = \frac{U_{\mathrm{dc\_}A} + U_{dc\ \_B} + U_{dc\ \_C}}{3}, \tag{2}$$

$$r_X = \frac{U_{dc\ \_X}}{U_{dc\ \_ave}} (X = \mathrm{A}, \mathrm{B}, \mathrm{and C}). \tag{3}$$

The voltage-second balancing principle defined in [17] for a three-level NPC converter is still suitable for CHB. Assuming that the variables ($U_{\mathrm{dc\_Xn}}$, T_{Xn}) remain constant within T_s, the volt-second product formula can be represented as follows:

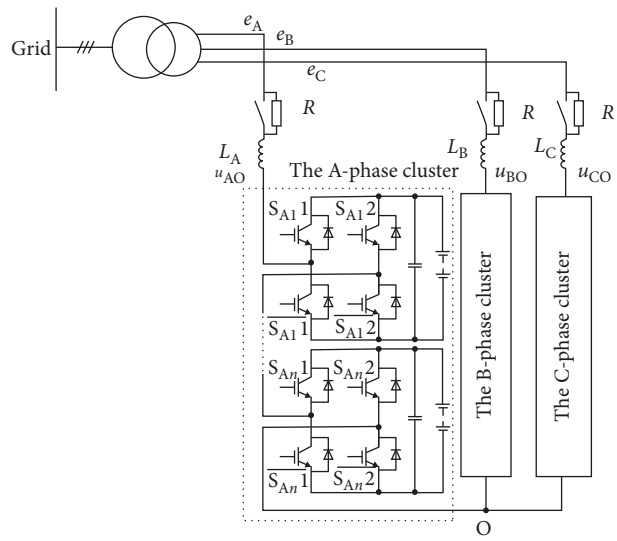

Figure 1: Circuit of the cascaded H-bridge converter.

$$\begin{aligned} u^*_{X\_ref} \cdot T_s &= \sum_{1}^{n} S_{Xn} \cdot U_{dc\ \_Xn} \cdot T_{Xn} + u_z \cdot T_S \\ &= U_{dc\ \_X} \cdot T_X + u_z \cdot T_s, \end{aligned} \tag{4}$$

where $u^*_{X\_\mathrm{ref}}$ stands for the three-phase reference voltages, T_s is the switching period, u_z is the equivalent zero-sequence voltage, T_X is the duration time of each phase, and T_{Xn} is the duration time of each submodule. ($S_{Xn} = S_{Xn1} - S_{Xn2}$) is the switching functions of each submodule, and $S_{Xni} = 0,1$ ($i = 1,2$).

To simplify the calculation process, duty cycle D_X is adopted instead of the duration time. The voltage-second balance in (4) can be rewritten as follows:

$$D_X = \frac{\frac{X}{T}}{T_s} = D^0_X - \Delta D_X = \left(\frac{1 - \mathrm{Sgn}\left(u^*_{X\_ref}\right)}{2} + \frac{u^*_{X\_ref}}{U_{dc\ \_X}} \right) - \frac{1}{r_X} \Delta D, \tag{5}$$

$$\begin{bmatrix} D_{\mathrm{A}_1} \\ D_{\mathrm{B}_1} \\ D_{\mathrm{C}_1} \end{bmatrix} = \begin{bmatrix} D_{\mathrm{A}_2} \\ D_{\mathrm{B}_2} \\ D_{\mathrm{C}_2} \end{bmatrix} = \cdots = \begin{bmatrix} D_{\mathrm{A}_n} \\ D_{\mathrm{B}_n} \\ D_{\mathrm{C}_n} \end{bmatrix} = \begin{bmatrix} D_{\mathrm{A}} \\ D_{\mathrm{B}} \\ D_{\mathrm{C}} \end{bmatrix}, \tag{6}$$

where ΔD_X represents the correction value that is added to D^0_X. In order to achieve the frequency multiplier effect of cascade H-bridge, the carrier phase shift technology is adopted, so the duty cycle of each submodule is the same before submodule power control, as shown in (6).

It should be noted that the duty cycle of each submodule is equally distributed before the submodule power control, and it will be modified during the introduction of the SPCA to achieve the submodule power control.

2.2. Extending Linear Modulation Range. The maximum value of modulation index m under unequal DC sources is reduced due to the distorted hexagon. In fact, it cannot reach the maximum modulation index when the traditional

SVPWM method is used, and voltage distortion is not avoidable. The essence of the problem is that the partial vector is assigned to the wrong sector because of the simplified PWM strategy. It can be effectively solved by the proposed method based on state transition [17], to achieve the linear modulation range extension and the waveform quality improvement.

Assuming that $u^*_{X\_\mathrm{ref}}$ is defined as (7), where m is the modulation index. D_X can be acquired by substituting (7) into (5).

$$u^*_{X\_ref} = m\mathrm{U}_{dc\ \_ave}F_{\cos}, \tag{7}$$

$$D_X = \left[\frac{1-\mathrm{Sgn}\left(F_{\cos}\right)}{2} + \frac{1}{r_X}mF_{\cos}\right] - \frac{1}{r_X}\Delta D, \tag{8}$$

$$F_{\cos} = \left[\cos(\theta)\cos\left(\theta - \frac{2\pi}{3}\right)\cos\left(\theta + \frac{2\pi}{3}\right)\right]^T, \tag{9}$$

$$\mathrm{Sgn}(t) = \begin{cases} 1, t \geq 0 \\ -1, t < 0 \end{cases}. \tag{10}$$

In order to get the linear modulation, D_X should be in the range of 0 to 1. Thereby, the existence condition of ΔD can be expressed by inequality as follows:

$$r_X\frac{1-\mathrm{Sgn}\left(F_{\cos}\right)}{2} + mF_{\cos} - r_X \leq \Delta D \leq r_X\frac{1-\mathrm{Sgn}\left(F_{\cos}\right)}{2} + mF_{\cos}. \tag{11}$$

Thus, the maximum linear modulation index $m_{\max}$ derived in [17] can be expressed by

$$m_{\max} = \min\left(\frac{r_A}{\sqrt{3}/2}, \frac{r_B}{\sqrt{3}/2}, \frac{r_C}{\sqrt{3}/2}\right), \tag{12}$$

where $m_{\max}$ is decided by the minimum value of r_X. In a comprehensive analysis in [18], the state transition includes the following two categories:

$$\begin{cases} \text{if } u^*_{X\_ref} < 0 \text{ and } D_X > 1, D^S_X = {}^X_D - 1, \\ \text{if } u^*_{X\_ref} > 0 \text{ and } D_X < 0, D^S_X = {}^X_D + 1. \end{cases} \tag{13}$$

Accordingly, the range of D_X is extended to [−1 1] or [0 2], and the existence condition of ΔD can be expressed by inequality as follows:

$$mF_{\cos} - r_X \leq \Delta D \leq mF_{\cos} + r_X. \tag{14}$$

Through the state transition, the maximum value $m_{\max\_\mathrm{ST}}$ can be obtained as follows by solving inequality (14). Obviously, $m_{\max\_\mathrm{ST}}$ is determined by the medium and minimum voltage value.

$$m_{\max\ \_\mathrm{ST}} = \min\left(\frac{\mathrm{r}_A + \mathrm{r}_B}{\sqrt{3}}, \frac{\mathrm{r}_A + \mathrm{r}_C}{\sqrt{3}}, \frac{\mathrm{r}_B + \mathrm{r}_C}{\sqrt{3}}\right). \tag{15}$$

The upper and lower limits of ΔD can be defined as follows:

$$\Delta D_{\min\ \_ST} = \max m\cos\theta - r_A, m\cos\left(\theta - \frac{2\pi}{3}\right) - r_B, \quad m\cos\left(\theta + \frac{2\pi}{3}\right) - r_C, \tag{16}$$

$$\Delta D_{\max\ \_\mathrm{ST}} = \min\left(m\cos\theta + \mathrm{r}_A, m\cos\left(\theta - \frac{2\pi}{3}\right) + \mathrm{r}_B, m\cos\left(\theta + \frac{2\pi}{3}\right) + \mathrm{r}_C\right). \tag{17}$$

To meet the target of extending the linear modulation, ΔD in the whole range should satisfy constraint ΔD_{in} $[\Delta D_{\min} - \mathrm{ST}\ \Delta D_{\max\text{-}\mathrm{ST}}]$ in all six sectors.

3. Analysis of the Proposed Power Control Method

When the CHB has assumed the interfacing converter for a battery system, the submodules will generate unbalanced output power and DC voltages, which must be considered in practice. Aiming at the interphase power and submodule power distribution problem, a power control algorithm under unbalanced DC sources is proposed here, to achieve precise interphase and submodule power control and maintain three-phase output current balance.

3.1. Definition of Control-Period Power and Average Power in DC Links. Let f_{fund}, f_{carrier}, and f_{sample} represent the fundamental frequency of u^*_{Xref}, the carrier-wave frequency, and sampling frequency, respectively. For convenience, both the control period T_{control} and carrier-wave period are equal to the sampling period. Assuming that the variables (U_{dc_X}, i_X, D_X, and u^*_{Xref}) keep constant within T_{control}, the control period (CP) power p_X is given in the following equation:

$$p_X = U_{\mathrm{dc}\_X}i_X \cdot \left[\left(D^0_{\ X} - \frac{\Delta D}{r_X}\right) - \frac{1-\mathrm{sgn}\left(u^*_{\mathrm{Xref}}\right)}{2}\right], \tag{18}$$

where i_X represents the three-phase current.

If $\mathrm{sgn}(i_X) = \mathrm{sgn}(u^*_{\mathrm{Xref}})$, then $p_X > 0$, which means that the DC sources release the power in the controlling period; otherwise, the DC sources absorb power.

Within T_{fund}, the single-phase average DC-power (SPA) PX can be expressed as follows:

$$P_X = f_{\mathrm{fund}}\sum_{j=0}^{N} p_{Xj}, \tag{19}$$

where N refers to the ratios of $f_{\mathrm{control}}/f_{\mathrm{fund}}$.

The three-phase average DC-power, P_{ave}, can thus be derived as follows:

$$P_{\mathrm{ave}} = \frac{\left(P_{\mathrm{A}} + P_{\mathrm{B}} + P_{\mathrm{C}}\right)}{3}. \tag{20}$$

From (20), we know that average DC-power P_{ave} is determined by three-phase reference voltages and AC currents, not related to ΔD.

3.2. Computational Principle of SPA Power in DC Links. The concept of the sliding window is introduced in [19] to calculate the SPA power. The width of the sliding window is equal to N. The calculation of SPA power within the previous N control period has been derived (19). After the sliding window moves one step, the SPA power can be expressed by

$$P_X^{\text{current}} = P^X + f_{\text{fund}}\left(p_{X\_\text{in}} - p_{X\_\text{out}}\right). \tag{21}$$

Thus, the SPA power flowing though individual DC sources can be acquired in each controlling period. As we can see from (21), P_X^{current} is decided by P^X, $p_{X\text{-in}}$, and $p_{X\text{-out}}$, revealing that P_X^{current} can be adjusted by ΔD in the current controlling period.

3.3. Proposed Unbalanced DC-Power Control Method. The adjustable DC-power ΔP_X within one controlling period is defined by

$$\Delta p_X = U_{\text{dc\_}X} i_X \cdot \frac{\Delta D}{r_X}. \tag{22}$$

Referring to (19), the adjustable DC-power ΔP_X within T_{fund} and the one in the current controlling period is expressed as follows:

$$\Delta P_X = f_{\text{fund}} \sum_{j=0}^{N} \Delta p_{Xj}, \tag{23}$$

$$\Delta P_X^{\text{current}} = \Delta P_X + f_{\text{fund}}\left(\Delta p_{X\_\text{in}} - \Delta p_{X\_\text{out}}\right). \tag{24}$$

In the generalized unbalanced case, k_X in the previous N controlling period can be rewritten as follows:

$$k_X = \frac{P_{\text{ave}} - \Delta P_X}{P_{\text{ave}}}. \tag{25}$$

The following steps outline the proposed active unbalanced DC-power control method when $k_X \neq \mathrm{k}^* X$. $\Delta P_{X\text{-in}}$ in the current controlling period should be changed to regulate the ratios.

3.3.1. Priority Control Phase Selection. The power generation ratio deviation is defined as $\Delta k_X = |k^* X\text{-}k_X|$. Since the phase with the largest value of Δk_X deviates worst, that phase will be set as the priority control phase. And the direction of ΔD will be decided by this one based on

$$\begin{aligned} &\text{if } \Delta k_{\text{A}} = \max\left(\Delta k_{\text{A}}, \Delta k_{\text{B}}, \Delta k_{\text{C}}\right), \Delta D \text{ decided by A,} \\ &\text{if } \Delta k_{\text{B}} = \max\left(\Delta k_{\text{A}}, \Delta k_{\text{B}}, \Delta k_{\text{C}}\right), \Delta D \text{ decided by B,} \\ &\text{if } \Delta k_{\text{C}} = \max\left(\Delta k_{\text{A}}, \Delta k_{\text{B}}, \Delta k_{\text{C}}\right), \Delta D \text{ decided by C.} \end{aligned} \tag{26}$$

3.3.2. Power Generation Ratio Comparison. By comparing k_X with k^*X, whether $\Delta P_X^{\text{current}}$ is increased or not can be determined. Furthermore, $\Delta P_{X\text{-in}}$ will be decided based on (24) as shown in the following equation:

$$\begin{cases} \text{if } k_X > k_X^*, \Delta P_X^{\text{current}} \downarrow \Rightarrow \Delta p_{X\_\text{in}} \downarrow, \\ \text{if } k_X \le k_X^*, \Delta P_X^{\text{current}} \uparrow \Rightarrow \Delta p_{X\_\text{in}} \uparrow. \end{cases} \tag{27}$$

3.3.3. Identify the Direction of ΔD in Current Controlling Period. Since the direction of $\Delta P_{X\text{-in}}$ has been decided by step 2, the variation direction of ΔD in the current controlling period is expressed by (28) based on (22). When substituting (19) and (18) into (24) gives equation (29), the relationship between kX and ΔD can be acquired, that is, the proper value of ΔD can be chosen to keep the three-phase power generation ratios under control accurately.

$$\begin{aligned} &\text{if } k_X > k_X^* \begin{cases} \text{if } \operatorname{sgn}(i_X) > 0, \Delta p_{X\_\text{in}} \downarrow \Delta D \uparrow \\ \text{if } \operatorname{sgn}(i_X) < 0, \Delta p_{X\_\text{in}} \downarrow \Delta D \downarrow \end{cases}, \\ &\text{if } k_X \le k_X^* \begin{cases} \text{if } \operatorname{sgn}(i_X) > 0, \Delta p_{X\_\text{in}} \uparrow \Delta D \downarrow \\ \text{if } \operatorname{sgn}(i_X) < 0, \Delta p_{X\_\text{in}} \uparrow \Delta D \uparrow \end{cases}, \end{aligned} \tag{28}$$

$$\Delta D = r_X \left\{ D_X^0 - \frac{1 - \operatorname{sgn}\left[u^*_{X\_\text{ref}}\right]}{2} - \left[\frac{N\left(k_X^* P_{\text{ave}} - P_X + p_{X\_\text{out}}\right]}{U_{\text{dc\_}X} i_X} \right\}. \tag{29}$$

3.3.4. Value Identification of ΔD in Current Controlling Period. According to the analysis mentioned in sectors A and B, the range of ΔD is $[\Delta D_{\min}\ \Delta D_{\max}]$. So ΔD is identified as follows:

$$\begin{aligned} &\text{if } \Delta D \uparrow \Delta D = \Delta D_{\max}, \\ &\text{if } \Delta D \downarrow \Delta D = \Delta D_{\min}, \end{aligned} \tag{30}$$

where the expressions of $\Delta D_{\max}$ and $\Delta D_{\min}$ are different in different cases in Section 3.

D_X, as derived from the steps above, can be used to generate the switching signals directly, if it satisfies constraint D_{X_in} [0 1]. Otherwise, the process of state transition in (13) is required. So far, the combination of both proposed algorithms (ST-PWM and IPCA) has been completed.

3.4. Control Flow of the Proposed Submodule Power Control Algorithm. Due to the series of structures of submodules in each phase, currents at the AC sides are identical. Conventional methods realize power control through superposing voltage components on the module reference voltage. In fact, submodule power control redistributes the output power of each module, which is related to the current direction, the switch state, and the duration time of the submodule. After the interphase power control, the duty cycle of each submodule defined as D_{Xn} in the following equation is a determined value:

$$D_{Xn} = D_{\cos} - \frac{1 - \operatorname{Sgn}\left(F_{\cos}\right)}{2}. \tag{31}$$

Following the SPCA, the DC-power p_{Xn} generated by the submodules within T_S is expressed as (32). The compensating value ΔD_{Xn} is introduced to redistribute the duty cycle of the submodules, and D_{Xn}^m is the value after compensating.

$$p_{Xn} = U_{\mathrm{dc\_}Xn} i_{Xn} \cdot [D_{Xn} - \Delta D_{Xn}] \cdot = U_{\mathrm{dc\_}Xn} i_{Xn} \cdot D_{Xn}^m. \quad (32)$$

In order to realize accurate individual submodule power control, the power generation ratios per module l_{Xn} are defined as (33), where P_X stands for the DC power per phase. l_{Xn} must satisfy the equality as follows:

$$l_{Xn} = \frac{P_{Xn}}{P_X}, \quad (33)$$

$$\sum_{n=1}^{M} l_{Xn} = \frac{P_{X1} + \cdots + P_{Xn}}{P_X} = 1, \quad (34)$$

where P_{Xn} represents the DC-power generated by each module.

Based on (21), P_{Xn} can be updated as follows:

$$p_{Xn\_\mathrm{in}} = N\left(P_{Xn}^* - P_{Xn}\right) + p_{Xn\_\mathrm{out}}. \quad (35)$$

Submitting (35) into (32) gives equation (36), ΔD_{Xn} can be acquired to control the distribution of submodule power:

$$\Delta D_{Xn} = D_{Xn} - \frac{Nl\left(_{Xn}^{*} P_X - P_{Xn} + p_{Xn\_\mathrm{out}}\right)}{U_{\mathrm{dc\_}Xn} i_{Xn}}. \quad (36)$$

The correction ΔD_{Xn} should satisfy constraint (37), when $(D_X - \Delta D_{Xn}(k))_{in}$ [−1 1].

$$D_X^{\mathrm{sum}} - 1 \le \Delta D_{Xn} \le 1 + D_X^{\mathrm{sum}}. \quad (37)$$

When it is stable in interphase power control, the power of each phase is constant, that is, $P_{Xn}^* = P_{Xn}^{\mathrm{old}}$. Therefore, the sum of ΔD_{Xn} of each phase is equal to zero. In other words, the duty cycle correction injected in each module can achieve submodule power control without influencing the interphase power control.

$$\sum_{n=1}^{M} \Delta D_{Xn} = \sum_{n=1}^{M} \left(D_X^{\mathrm{sum}} - \frac{N\left(P_{Xn}^* - P_{Xn}\right) + p_{Xn\_\mathrm{out}}}{U_{\mathrm{dc\_}Xn} i_{Xn}} \right) = 0. \quad (38)$$

Once ΔD_{Xn} reaches its limit, (38) does not work. To avoid an impact on interphase power control, the correction of the last module must be obtained as follows:

$$\Delta D_{XM} = -\sum_{n=1}^{M-1} \Delta D_{Xn}. \quad (39)$$

Finally, in SVPWM applications, the duty cycle needs to be converted to duration time as follows:

$$T_{Xn} = D_{Xn} \cdot T_S. \quad (40)$$

3.5. Loss Calculation and Blocking Voltage Stress. The loss is mainly determined by the IGBT conduction loss $P_{\mathrm{con,T}}$ and switching loss $P_{\mathrm{sw,T}}$ and the diode conduction loss and reverse recovery loss.

Table 1: Parameter settings for simulation.

Parameter	Value
Voltage of battery cells	12 V
DC-link capacitor	1,200 μF
Resistive-inductive load	10 Ω, 4 mH
Switching frequency	8 kHz
Chain number per phase	2

As to the IGBT, the total loss P_{T} can be written as follows:

$$P_T = P_{\mathrm{con},T} + P_{sw,T},$$
$$P_{\mathrm{con},T} = v_{0,T} I + r_T I^2. \quad (41)$$

where $v_{0,\mathrm{T}}$ is the initial saturation voltage drop of IGBT and r_{T} is the conduction resistance of IGBT.

$$P_{\mathrm{sw,T}} = f_{\mathrm{sw}} E_{\mathrm{sw,T}}(I), \quad (42)$$

where f_{sw} is the switching frequency and $E_{\mathrm{sw,T}}(I)$ is the switching energy of IGBT.

As to the diode, the total loss P_{D} can be written as follows:

$$P_D = P_{\mathrm{con},D} + P_{\mathrm{rec},D},$$
$$P_{\mathrm{con},D} = v_{0,D} I + r_D I^2. \quad (43)$$

where $v_{0,\mathrm{D}}$ is the initial saturation voltage drop of the diode and r_{D} is the conduction resistance of the diode.

$$P_{\mathrm{rec,D}} = f_{\mathrm{sw}} E_{\mathrm{rec,D}}(I), \quad (44)$$

where f_{sw} is the switching frequency and $E_{\mathrm{rec,D}}(I)$ is the reverse recovery energy of the diode.

Blocking stress varies with the DC link voltages across the power switches. As to the high power converter design, we should obtain parasitic inductances in each loop in order to minimize the turn-off voltage spike of the IGBT.

3.6. Stability Analysis. The DC-power control strategy is an open-loop control. The DC-power references are used as the command to modify the correction value ΔD. So there is no stability problem. The converter is controlled as a grid-connect converter, and a voltage and current double closed-loop control are adopted. This may raise stability problems. The voltage and current regulators used are all PI controllers. To acquire the stable system, the current inner loop is set into a typical type I system; then the bandwidth of the outer loop is tuned lower then inner loop; and it is set into a typical type II system.

4. Simulation Verification

The simulation model of the inverter is set up to analyze the relationship between voltage-imbalance coefficients and modulation index and the relationship between power generation ratios and modulation index, which can provide a

Table 2: Battery cell settings for simulation and experiment.

DC-source voltage of each submodule					
Phase A		Phase B		Phase C	
U_{dc_A1}	U_{dc_A2}	U_{dc_B1}	U_{dc_B2}	U_{dc_C1}	U_{dc_C2}
48 V	24 V	48 V	60 V	48 V	96 V

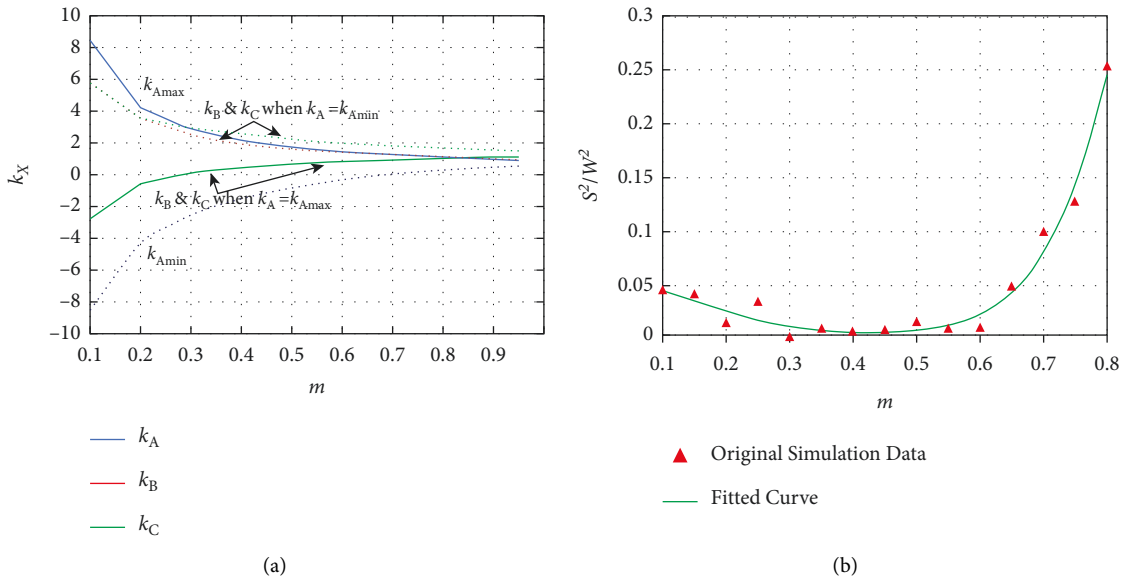

(a) (b)

Figure 2: Control performance of output power generation when $r_A = 2/3$, $r_B = 1$ $r_C = 4/3$, $R_X = 10\,\Omega$, and $L_X = 4$ mH: (a) relationship of m and $k_{Amax/min}$ and (b) trend of three-phase variance S^2 with m.

reference for the grid-connected systems. The proposed ST-PWM strategy is simulated in MATLAB/Simulink to control a three-phase five-level CHBI. The simulated parameters are listed in Table 1. And the battery cells are set as in Table 2.

4.1. Control Performance of the Proposed ST-PWM Strategy with IPCA. To evaluate the performance of a proposed ST-PWM strategy with IPCA, the simulation is carried out with the battery cells settings in Table 2. Therefore, the interphase voltage-imbalance coefficients are $r_A = 2/3$, $r_B = 1$, and $r_C = 4/3$. In this case, the maximum modulation index m_{max_ST} is 0.96 based on (15). To simplify the relationship between m and $k_{Amax/min}$, phase A is set as the priority control phase at all times. This operation means that ΔD is decided by the power generation ratio k_A. Figure 2(a) is drawn to describe the trends when $r_A = 2/3$, $r_B = 1$, $r_C = 4/3$, $R_X = 10\,\Omega$, and $L_X = 4$ mH. k_{Amax} decreases as the modulation index m increases. Meanwhile, k_B and k_C increase as m increases when $k_A = k_{Amax}$. The trends of k_B and k_C, when $k_A = k_{Amin}$, are opposite to when $k_A = k_{Amax}$. Noting that the value of k_X can be negative, which means the corresponding phase will absorb power from the system. The ranges of k_X become smaller when $m \in [0.7\ 0.96]$ as shown in Figure 2(a).

Figure 2(b) shows the trend of three-phase variance S^2 defined in (44), where P_{X_real} and $P_{X\_theoretical}$ represent the real and theoretical DC-power generated by DC sources per phase, respectively. This figure is obtained under conditions of $(k_A = k_B = k_C = 1)$, $(r_A = 2/3, r_B = 1, r_C = 4/3)$, and $R_X = 10\,\Omega$, and $L_X = 4$ mH. Obviously, most values of S^2 with the proposed method are smaller than 0.25 W^2 in simulation, which suggests that the power control performance of the proposed ST-PWM strategy is accurate. The simulation results show that the proposed method is (1) capable of providing more accurate results for DC-power control and (2) suitable for DC-power control under unbalanced DC sources, even under the severely unbalanced voltage condition.

Table 3: Parameters in the simulation.

Parameters	Value
Rated power (VA)	750
Rated line-to-line RMS voltage (V)	95
Switching frequency (kHz)	8
DC-link capacitors (μF)	1,200
Filtering inductor (mH)	4

$$S^2 = \frac{1}{3} \sum_{X=A,B,C} \left(P_{X\_real} - P_{X\_theoretical}\right)^2. \quad (45)$$

4.2. Control Performance of Proposed Power Control Methods. To evaluate the proposed power control methods on grid-tied conditions, the simulation combined with IPCA and SPCA is implemented with the parameters in Table 3. Figure 3 shows the control block diagram of the grid-

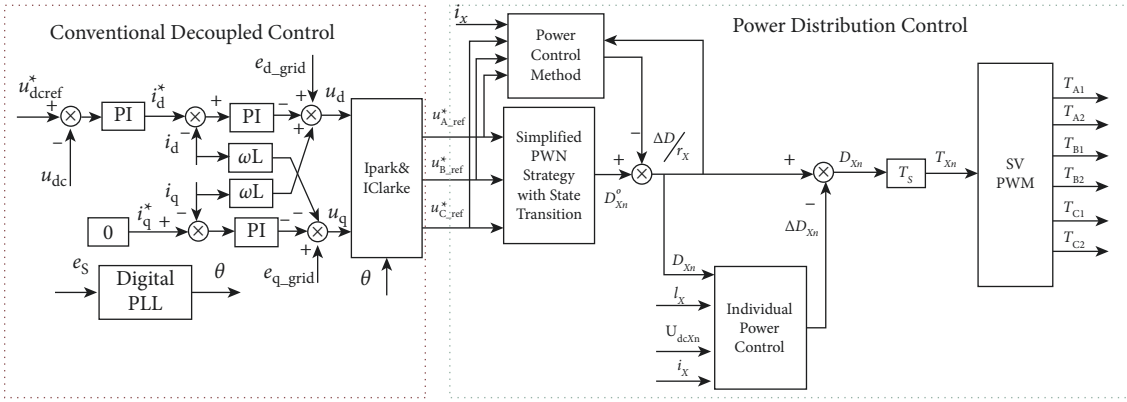

Figure 3: Control block diagram of the grid-connected inverter system.

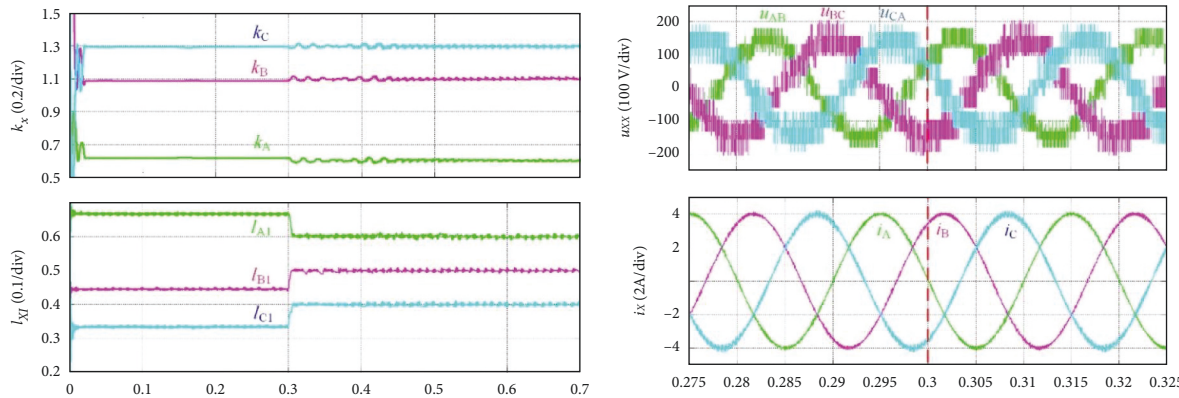

Figure 4: The simulation results with $r_A = 2/3$, $r_B = 1$, and $r_C = 4/3$: (a) waveforms of power generation ratios k_X and submodule power generation ratios l_{X1} and (b) waveforms of line voltage u_{XX} and currents i_X.

connected inverter with proposed methods. The control is divided into two subcontrols: (1) conventional decoupled control based on the d-q rotational frame and (2) power-distribution control. Moreover, the power distribution control is divided into the extension of modulation index, interphase power control, and submodule power control. First, three-phase voltage references acquired by conventional decoupled control are used for calculating the duration time. Then the correction value ΔD derived from the IPCA is added to the duty cycle of each phase to control the power distribution among the three phases. Once corrected D_X falls outside of [0 1], the state transition algorithm is needed to extend the linear modulation range. At last, the compensating value ΔD_{Xn} is added to the duty cycle of each submodule to realize the submodule power control.

Figure 4 shows interphase power control and submodule power control, where the three-phase power generation ratios keep constant as $k^*A = 0.6$, $k^*B = 1.1$, and $k^*C = 1.3$ in the whole period and the submodule power generation ratios are set as $l_{A1} = 0.6$, $l_{B1} = 0.5$, $l_{C1} = 0.4$ after 0.3 s. Figure 5(a) shows that interphase power and submodule power can be accurately controlled after introducing IPCA and SPCA, and the submodule power control has little negative impact on interphase power control. It should be noted that the

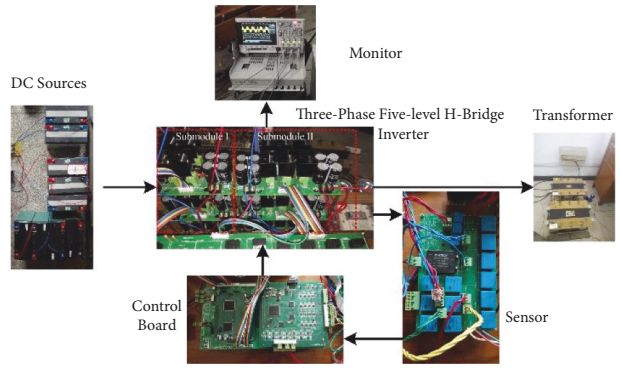

Figure 5: Experimental setup.

submodule power is allocated with the submodule voltage as $l_{A1} = 2/3$, $l_{B1} = 4/9$, and $l_{C1} = 1/3$ when the submodule power control algorithm is absent. From Figure 4(b), it is obvious that balanced AC currents can be achieved, even when submodule power generation ratios are changed.

5. Experimental Verification

A 750 VA three-phase five-level CHB inverter system has been developed in our laboratory to verify the performance

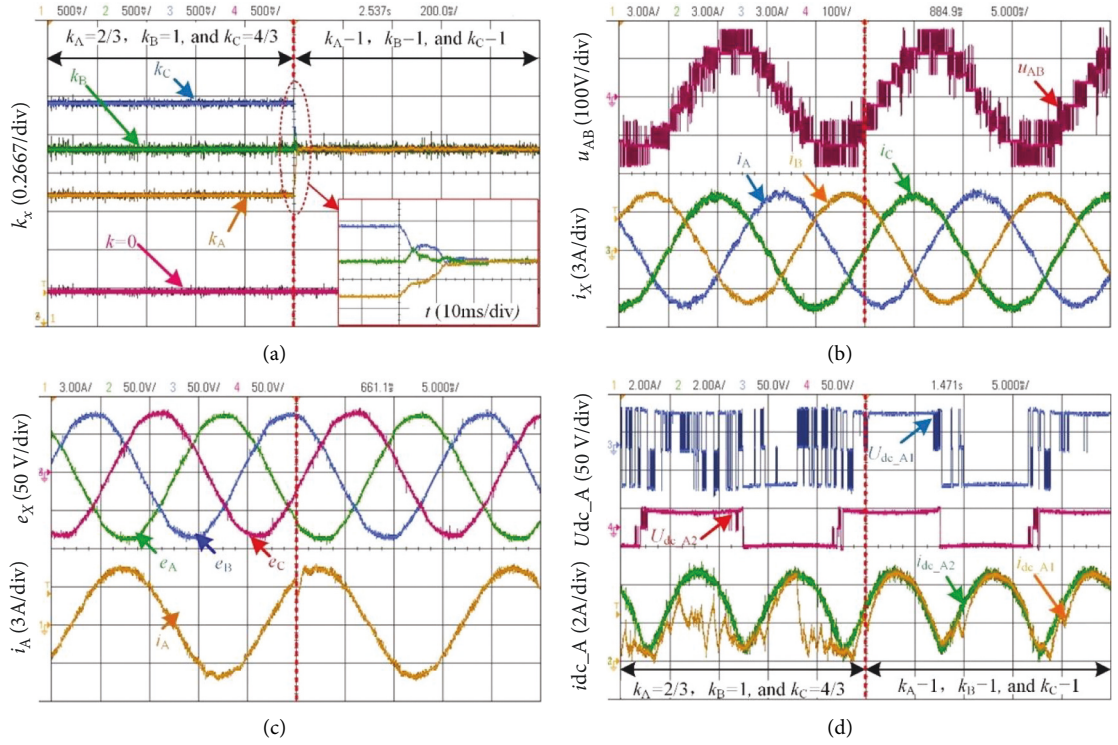

FIGURE 6: The experimental results with $r_A = 2/3$, $r_B = 1$, and $r_C = 4/3$: (a) waveforms of power generation ratios k_X, (b) waveforms of line voltage u_{AB}. and currents i_X, (c) phase current i_A and the grid voltage e_X, and (d) submodule DC side currents and voltages of phase A.

of the proposed method as depicted in Figure 5. Two groups of experiments are implemented under voltage-imbalance conditions. A three-phase downscaled grid-connected converter is constructed. The corresponding experimental environment and configuration are shown in Figure 1. The parameters are the same as the simulation in Table 3, and the switching frequency is 8 kHz. It should be noted that the H-bridge unit is coupled with a lead-acid battery to provide power to the grid rather than a solar power unit, due to our limited experimental conditions. A DC-DC step-up converter, which is usually required for MPPT of solar PV systems, is omitted in the experiments due to the use of the battery. The proposed algorithms are implemented in TMS320F28335 with Xilinx FPGA boards.

5.1. Control Performance of Interphase Power Generation. Experiments with $r_A = 2/3$, $r_B = 1$, and $r_C = 4/3$ were conducted to evaluate the dynamic performances of the proposed modulation strategy when interphase power generation ratios changed. In Figure 2(a), the maximum value of k_A is 1.057 when $m = 0.89$. Hence, the reference power generation ratios can be set as follows: $k^*A = 2/3$, $k^*B = 1$, and $k^*C = 4/3$ in the first semiperiod and $k^*A = k^*B = k^*C = 1$ in the second semiperiod. Figure 6(a) gives the overall waveforms of power generation ratios k_X, which reach their expected values precisely in the whole period. Besides, the detailed view shows that the transient process lasts about 20 ms. It requires one fundamental period to get a complete update of the average power. Figure 6(b) shows the line voltages u_{AB} and three-phase currents. It is obvious that balanced AC currents can be achieved when power generation ratios change, and this change has little effect on the AC currents. Figure 6(c) shows grid phase voltage e_X and inverter current i_A. Figure 6(d) shows the waveforms of the submodule's DC-side current and phase A voltage. From the voltage and current waveforms of each module, we can see that module 2 is always in the state of maximum power output, while module 1 is in the supplementary state. The DC side current has changed significantly before and after the interphase power switching, Thus, the effectiveness of the proposed power control is verified.

5.2. Control Performance of Submodule Power Generation. Experiments with submodule power control with $r_A = 2/3$, $r_B = 1$, and $r_C = 4/3$ are conducted to evaluate the performance of the proposed modulation strategy when power generation ratios changed. Figure 7(a) provides the overall waveforms of power generation ratios k_X, which remains constant during the entire period. Figure 7(b) shows the submodule power generation ratios. The submodule power is allocated with the submodule voltage when there is no submodule power control. As can be seen from Figure 7(b), the submodule power generation ratios reach the expected value over a short period of time. Grid phase voltage e_X and inverter current i_A are shown in Figure 7(c). Figure 7(d)

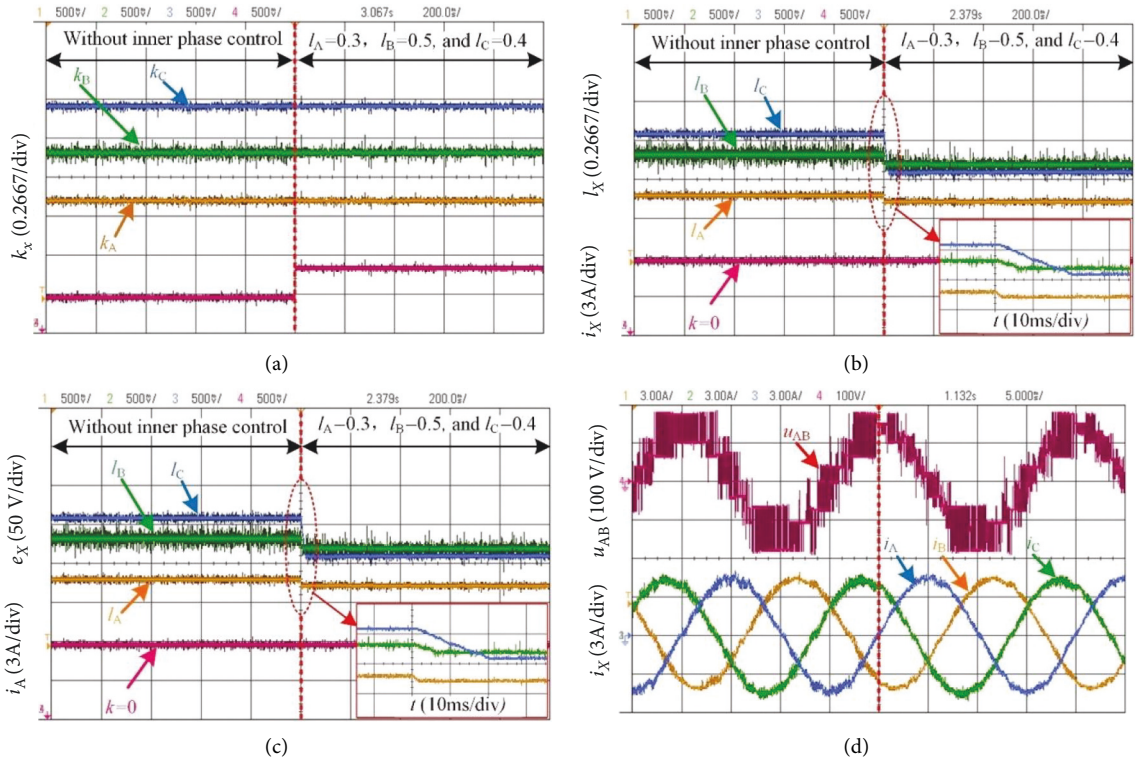

Figure 7: The experimental results in with $r_A = 2/3$, $r_B = 1$, and $r_C = 4/3$: (a) waveforms of power generation ratios k_X, (b) waveforms of submodule power generation ratios l_{Xn}, (c) phase current i_A and the grid voltage e_X, and (d) waveforms of line voltage u_{XX} and currents i_X.

shows line voltage u_{AB} and three-phase currents in the switching process, which indicates that the submodule power control has little or no effect on the AC currents.

6. Conclusion

This paper has proposed a novel power control method for the CHB with unbalanced DC sources. First, the limitation of the modulation index was deeply analyzed to acquire the maximum linear modulation index. Then, the range of correction values is derived in detail, and the modulation index is extended by the maximum value with the ST-PWM strategy. Meanwhile, interphase and submodule power control algorithms have been proposed to maintain power generation ratios at the expected values. For simulation and experimental verification, the proposed control algorithm has been applied to a five-level CHB, which has achieved balanced grid-side currents and accurate power control. In order to acquire precise DC-power control, the switching frequency will be higher than traditional control strategies such as carrier phase-shifting control. So the efficiency of the system will be reduced slightly.

Data Availability

The simulation model and experimental setup are established and tested by our research group in the laboratory. We would like to share all our simulation and experiment data with others through e-mail 59546461@qq.com. Xia, the first author, can provide data details and necessary explanations to querists.

Conflicts of Interest

The authors declare that they have no conflicts of interest.

Acknowledgments

This work was supported by the youth fund of the Foundation Research Project of Jiangsu Province (BK20160219).

References

[1] S. Kouro, M. Malinowski, K. Gopakumar et al., "Recent advances and industrial applications of multilevel converters," *IEEE Transactions on Industrial Electronics*, vol. 57, no. 8, pp. 2553–2580, 2010.

[2] A. Marzoughi, R. Burgos, D. Boroyevich, and Y. Xue, "Investigation and Comparison of Cascaded H-Bridge and Modular Multilevel Converter Topologies for Medium-Voltage Drive Application," in *Proceedings of the Industrial Electronics Society, IECON 2014 - 40th Annual Conference of the IEEE*, pp. 1562–1568, Dallas, TX, USA, November, 2014.

[3] N. Salehi, H. Martínez-García, and G. Velasco-Quesada, "Modified cascaded Z-source high step-up boost converter," *Electronics*, vol. 9, no. 11, p. 1932, 2020.

[4] M. Malinowski, K. Gopakumar, J. Rodriguez, and M. A. Pérez, "A survey on cascaded multilevel inverters," *IEEE Transactions on Industrial Electronics*, vol. 57, no. 7, pp. 2197–2206, Jul.2010.

[5] J. Aguayo-Alquicira and I. Vásquez-Libreros, "Reconfiguration strategy for fault tolerance in a cascaded multilevel inverter using a Z-source converter," *Electronics*, vol. 10, no. 5, p. 574, 2021.

[6] Z. Zheng, K. Wang, L. Xu, and Y. Li, "A hybrid cascaded multilevel converter for battery energy management applied in electric vehicles," *IEEE Transactions on Power Electronics*, vol. 29, no. 7, pp. 3537–3546, 2014.

[7] L. Liu, H. Li, S.-H. Hwang, and J.-M. Kim, "An energy-efficient motor drive with autonomous power regenerative control system based on cascaded multilevel inverters and segmented energy storage," *IEEE Transactions on Industry Applications*, vol. 49, no. 1, pp. 178–188, 2013.

[8] G. Farivar, B. Hredzak, and V. G. Agelidis, "A DC-side sensorless cascaded H-bridge multilevel converter-based photovoltaic system," *IEEE Transactions on Industrial Electronics*, vol. 63, no. 7, pp. 4233–4241, 2016.

[9] B. Xiao, L. Hang, J. Mei, C. Riley, L. M. Tolbert, and B. Ozpineci, "Modular cascaded H-bridge multilevel PV inverter with distributed MPPT for grid-connected applications," *IEEE Transactions on Industry Applications*, vol. 51, no. 2, pp. 1722–1731, 2015.

[10] Y. Yu, G. Konstantinou, B. Hredzak, and V. Agelidis, "Optimal Zero Sequence Injection in Multilevel Cascaded H-Bridge Converter under Unbalanced Photovoltaic Power Generation," in *Proceedings of the International Power Electronics Conference*, pp. 1458–1465, Hiroshima, Japan, May, 2014.

[11] Y. Yu, G. Konstantinou, B. Hredzak, and V. G. Agelidis, "Power balance of cascaded H-bridge multilevel converters for large-scale photovoltaic integration," *IEEE Transactions on Power Electronics*, vol. 31, no. 1, pp. 292–303, 2016.

[12] L. Maharjan, S. Inoue, H. Akagi, and J. Asakura, "State-of-Charge (SOC)-Balancing control of a battery energy storage system based on a cascade PWM converter," *IEEE Transactions on Power Electronics*, vol. 24, no. 6, pp. 1628–1636, 2009.

[13] L. J. Kere, M. L. Doumbia, S. Kelouwani, and K. Agbossou, "Cascaded H-bridge multilevel converter for electric vehicle speed control," in *Proceedings of the Vehicle Power and Propulsion Conference (VPPC)*, pp. 1–6, Montreal, QC, Canada, Octobar, 2015.

[14] K. Kandasamy, M. Vilathgamuwa, and K. J. Tseng, "Intermodule state-of-charge balancing and fault-tolerant operation of cascaded H-bridge converter using multi-dimensional modulation for electric vehicle application," *IET Power Electronics*, vol. 8, no. 10, pp. 1912–1919, 2015.

[15] L. M. Tolbert, J. N. Chiasson, K. J. McKenzie, and D. Zhong, "Control of cascaded multilevel converters with unequal voltage sources for HEVs," in *Proceedings of the Electric Machines and Drives Conference, 2003. IEMDC'03*, pp. 663–669, IEEE International, Madison, WI, USA, June, 2003.

[16] T. Zhao, G. Wang, S. Bhattacharya, and A. Q. Huang, "Voltage and power balance control for a cascaded H-bridge converter-based solid-state transformer," *IEEE Transactions on Power Electronics*, vol. 28, no. 4, pp. 1523–1532, 2013.

[17] Z. Ye, T. Wang, S. Mao et al., "A PWM strategy based on state transition for cascaded H-bridge inverter under unbalanced DC sources," *IEEE Journal of Emerging and Selected Topics in Power Electronics*, vol. 8, no. 2, pp. 1686–1700, 2020.

[18] Y. Cho, T. LaBella, J.-S. Lai, and M. K. Senesky, "A carrier-based neutral voltage modulation strategy for multilevel cascaded inverters under unbalanced DC sources," *IEEE Transactions on Industrial Electronics*, vol. 61, no. 2, pp. 625–636, 2014.

[19] Z. Ye, Y. Xu, X. Wu, G. Tan, X. Deng, and Z. Wang, "A simplified PWM strategy for a neutral-point-clamped (NPC) three-level converter with unbalanced DC links," *IEEE Transactions on Power Electronics*, vol. 31, no. 4, pp. 3227–3238, 2016.